

# Different critical behaviors in cubic to trigonal and tetragonal perovskites

Amnon Aharony,<sup>1,\*</sup> Ora Entin-Wohlman,<sup>1,†</sup> and Andrey Kudlis<sup>2,‡</sup>

<sup>1</sup>*School of Physics and Astronomy, Tel Aviv University, Tel Aviv 6997801, Israel*

<sup>2</sup>*ITMO University, Kronverkskiy prospekt 49, Saint Petersburg 197101, Russia*

(Dated: February 21, 2022)

Perovskites like  $\text{LaAlO}_3$  (or  $\text{SrTiO}_3$ ) undergo displacive structural phase transitions from a cubic crystal to a trigonal (or tetragonal) structure. For many years, the critical exponents in both these types of transitions have been fitted to those of the isotropic three-components Heisenberg model. However, field theoretical calculations showed that the isotropic fixed point of the renormalization group is unstable, and renormalization group iterations flow either to a cubic fixed point or to a fluctuation-driven first-order transition. Here we show that these two scenarios correspond to the cubic to trigonal and to the cubic to tetragonal transitions, respectively. In both cases, the critical behavior is described by slowly varying effective critical exponents, which exhibit universal features. For the trigonal case, we predict a crossover of the effective exponents from their Ising values to their cubic values (which are close to the isotropic ones). For the tetragonal case, the effective exponents can have the isotropic values over a wide temperature range, before exhibiting large changes en route to the first-order transition. New renormalization group calculations near the isotropic fixed point in three dimensions are presented and used to estimate the effective exponents, and dedicated experiments to test these predictions are proposed. Similar predictions apply to cubic magnetic and ferroelectric systems.

## I. INTRODUCTION

Perovskite materials exhibit intriguing physical properties, and have been extensively explored for both practical applications and theoretical modeling [1]. In particular, perovskites like  $\text{SrTiO}_3$  and  $\text{LaAlO}_3$  play important roles in modern solid state applications [2]. At high temperatures, perovskites usually have a cubic structure (left panel, Fig. 1). As the temperature  $T$  decreases, some perovskites undergo an antiferrodistortive structural transition from the cubic to a lower-symmetry structure, via a rotation of the oxygen (or fluorine) octahedra:  $\text{SrTiO}_3$ ,  $\text{KMnF}_3$ ,  $\text{RbCaF}_3$  and others undergo a cubic to tetragonal transition, see Fig. 1. The octahedra rotate around a cubic axis and the order-parameter vector  $\mathbf{Q}$  (aka the rotation vector) is along that axis (with a length proportional to the rotation angle). Similar rotations occur in double perovskites, e.g., the tetragonal to orthorhombic transition in  $\text{La}_2\text{CuO}_4$  [3]. In contrast, other perovskites, e.g.,  $\text{LaAlO}_3$ ,  $\text{PrAlO}_3$ , and  $\text{NdAlO}_3$ , undergo a cubic to trigonal transition, with  $\mathbf{Q}$  along one of the cubic diagonals.

The behavior of a system at the vicinity of its transition temperature  $T_c$  can be expressed by critical exponents. When the transition at  $T_c$  is continuous, the correlation length diverges as  $\xi \propto |t|^{-\nu}$  and the order-parameter approaches zero (for temperatures  $T < T_c$ ) as  $|\langle \mathbf{Q} \rangle| \propto |t|^\beta$ , where  $t = T/T_c - 1$ . The critical exponents  $\nu$  and  $\beta$  are expected to be universal, i.e., having the same values for many physical systems. The exponents describing other physical properties, e.g.,  $\alpha$  and  $\gamma$  for the

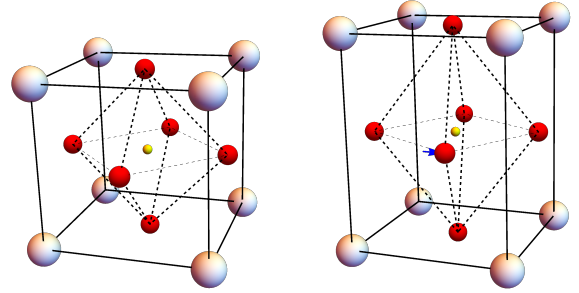


FIG. 1. (color online) The cubic (left) and tetragonal (right) unit cells in  $\text{SrTiO}_3$  (the latter shows only half the cell: neighboring cells rotate in opposite directions). Large, intermediate and small spheres correspond to Sr, O and Ti ions, respectively. The dashed lines represent the octahedra, which rotate around the vector  $\mathbf{Q}$ , lying along the vertical axis (the O ions in the central horizontal plane move as indicated by the arrow). When  $\mathbf{Q}$  is along a diagonal of the cube, the octahedra rotate around that diagonal, and the unit cell is stretched along  $\mathbf{Q}$ , causing a cubic to trigonal transition (as in  $\text{LaAlO}_3$ ).

specific heat and for the order parameter susceptibility, are obtained via scaling relations,  $d\nu = 2 - \alpha = 2\beta + \gamma$ , where  $d$  is the dimensionality.

The  $T$ -dependence of the order-parameters of  $\text{SrTiO}_3$  and  $\text{LaAlO}_3$  had been measured by Müller and Berlinger [4], who obtained a collapse of the scaled order-parameters in both materials onto a single line, showing a crossover from the mean-field exponent  $\beta_{MF} = 1/2$ , valid relatively far away from  $T_c$  (i.e., at relatively large  $|t|$ ) to an apparently universal critical exponent  $\beta_c = 0.33 \pm 0.02$  close to  $T_c$ . Consequently, it was concluded erroneously that both materials share the same exponents, and so belong to the *same universality class* and have the same

\* aaharonyaa@gmail.com

† orawohlman@gmail.com

‡ andrewkudlis@gmail.com

critical behavior. In fact it turned out that both samples were *single domains*, due to a uniaxial anisotropy caused by polishing [5]. Therefore both systems ordered along a *single* axis, and the data were consistent with Ising ( $n = 1$ , a single-component order-parameter) exponents [6–8]. Later experiments gave a wide range of results, e.g.  $\beta \simeq 0.40 \pm 0.03$ ,  $1/3$ ,  $0.27$ ,  $0.17 \pm 0.02$  for  $\text{SrTiO}_3$  [9],  $\text{KMnF}_3$  [10],  $\text{RbCaF}_3$  and  $\text{NaNbO}_3$  [11], respectively. Furthermore, some experiments hint that  $\text{SrTiO}_3$  may be close to a tricritical point [12–14], while both  $\text{RbCaF}_3$  and  $\text{KMnF}_3$  have first-order transitions [15, 16]. More experiments are reviewed e.g. in Refs. 17–19.

Here we show theoretically that the cubic to trigonal and the cubic to tetragonal phase transitions do not share the same critical behavior. In fact these two transitions are characterized by different behaviors of the renormalization-group (RG) iterations. We find that systems undergoing a cubic to trigonal transitions have second-order transitions, with the universal critical exponents of the cubic fixed point (FP). However, since the cubic and the isotropic fixed points turn out to be very close to each other (see below), it is indeed difficult to distinguish between their asymptotic critical exponents even without any uniaxial symmetry breaking. As we show, these asymptotic exponents are expected only very close to  $T_c$ . For a large range of  $t$  we predict *effective exponents*, which vary with  $t$ . In contrast, the cubic to tetragonal transitions become fluctuation-driven first-order at small  $|t|$ , with different effective exponents over an intermediate range of  $t$ . These effective exponents are characterized by the isotropic fixed point, which dominates the crossover to the first-order transition. This conclusion extends to quite a number of other systems as well.

Our predictions for the effective exponents come from a novel way to obtain analytic solutions to the RG recursion relations in the vicinity of the isotropic and cubic fixed points. After a short review of the theory of the RG on cubic systems in Sec. II, Sec. III presents our new calculation. Our predictions are compared with the above experimental information in Sec. IV, where we also propose dedicated measurements to test our results and list other cubic systems, which are expected to exhibit similar behaviors. Section V contains our conclusions. The Appendices describe the resummation technique and the analytic solution of the recursion relations.

## II. THE RENORMALIZATION GROUP ON CUBIC SYSTEMS

Fifty years ago, Wilson [20] showed that at  $T$  very close to  $T_c$  the short-length details can be eliminated on scales below  $1/e^\ell$  ( $\ell$  counts the number of iterations in the elimination process), and that rescaling the unit length by the factor  $e^\ell$  yields a renormalized effective (dimensionless) Hamiltonian (or free-energy density)  $\bar{\mathcal{H}}(\ell)$ , which ‘flows’ in the space spanned by all such Hamiltonians.

These flows represent the RG. Critical points are associated with fixed points of these flows, which are invariant under the RG iterations. Near a fixed point, the singular part of the corresponding free-energy density obeys the homogeneous scaling form

$$\begin{aligned} \mathcal{F}(\{\mu_i\}) &= e^{-d\ell_f} \mathcal{F}(\{\mu_i(0)e^{\lambda_i\ell_f}\}) \\ &\equiv |t|^{d\nu} \mathcal{W}(h|t|^{-\nu\lambda_2}, \mu_3(0)|t|^{-\nu\lambda_3}, \dots), \end{aligned} \quad (1)$$

where the  $\mu_i(0)$ ’s are parameters that measure deviations from the fixed point, and the  $\lambda_i$  are exponents describing their variation as function of  $\ell$ . The first two parameters are the temperature  $\mu_1 = t$  and the ordering field  $\mu_2 = h$ . Continuing the RG flow until  $\xi(\ell_f) = \xi(0)e^{-\ell_f} \sim 1$ , with  $\xi(0) \sim |t(0)|^{-\nu}$ , yields  $\nu = 1/\lambda_1$ . Derivatives of  $\mathcal{F}$  w.r.t.  $t$  and  $h$  yield the critical exponents for the measurable quantities, e.g. the scaling relations  $\beta = \nu(d - \lambda_2)$ ,  $\gamma = \nu(d - 2\lambda_2)$  and  $\alpha = 2 - d\nu$ . The exponents and the scaling function  $\mathcal{W}$  for systems near a specific FP are fully determined by the FP itself, and not by the initial effective Hamiltonian, which encompasses the short-scales behavior. Therefore they are universal [21–24]. All the physical systems which flow to that FP then belong to its universality class, and exhibit the same critical exponents. A stable fixed point has only two relevant variables,  $t$  and  $h$ , with  $\lambda_1, \lambda_2 > 0$ . All the other parameters are irrelevant, with  $\lambda_i < 0$ . In contrast, when a third parameter,  $\mu_3$ , is also relevant,  $\lambda_3 > 0$ , the fixed point is unstable, and the RG trajectories flow to another, stable, fixed point, via a crossover region, or flow to a region where the renormalized Hamiltonian has a first order transition.

The RG analysis of cubic systems has been mainly based on the Landau theory [25, 26], which expands the free-energy density in powers of the (small) order-parameter components  $Q_i$  ( $i = 1, 2, \dots, n$ ). The terms in this expansion are determined by the symmetries of the system *above the transition*. For the isotropic  $n$ -component order-parameter vector  $\mathbf{Q}$ , this free-energy is  $U_0(\mathbf{Q}) = r|\mathbf{Q}|^2/2 + u|\mathbf{Q}|^4 + \mathcal{O}[|\mathbf{Q}|^6]$ , where  $u$  is a system-dependent parameter, while  $r = T/T_c^{\text{MF}} - 1$ , with the mean-field transition temperature  $T_c^{\text{MF}}$  (the parameter  $t$ , mentioned above, contains the downwards shift from  $T_c^{\text{MF}}$  to  $T_c$  by the fluctuations). The cubic symmetry is characterized by adding the term  $U_v(\mathbf{Q}) = v\sum_{i=1}^n Q_i^4$  to the free energy, with  $v$  a system-dependent coefficient [27, 28]. Long wave-length fluctuations in  $\mathbf{Q}(\mathbf{r})$  are introduced via a gradient term [29],  $|\nabla\mathbf{Q}(\mathbf{r})|^2$ , whose coefficient is normalized to 1. The effective Hamiltonian is then written as  $\int d^d r \bar{\mathcal{H}}(\mathbf{r})$ , where

$$\bar{\mathcal{H}}(\mathbf{r}) \equiv |\nabla\mathbf{Q}(\mathbf{r})|^2/2 + U_0[\mathbf{Q}(\mathbf{r})] + U_v[\mathbf{Q}(\mathbf{r})]. \quad (2)$$

In the absence of the ordering field  $h$ , the parameters which flow under the RG iterations are  $r$ ,  $u$  and  $v$ .

The Wilson-Fisher RG at  $d = 4 - \epsilon$  is performed in Fourier space, eliminating large momentum (small length scale) components of the order-parameter [21, 30]. As we discuss below, it is not trivial to extrapolate the results

to  $d = 3$ , i.e.,  $\epsilon = 1$ . Generally, the recursion relations in the  $u - v$  plane have the form

$$\frac{\partial u}{\partial \ell} = \bar{\beta}_u[\epsilon, u(\ell), v(\ell)], \quad \frac{\partial v}{\partial \ell} = \bar{\beta}_v[\epsilon, u(\ell), v(\ell)], \quad (3)$$

and the  $\bar{\beta}$  functions (not to be confused with the critical exponent  $\beta$ ) are expanded in powers of their arguments. The fixed points  $u^*, v^*$  are found as the zeroes of these functions, with values which are series in  $\epsilon$ . For  $v = 0$ , this procedure gives two FP's, one at  $u_G^* = 0$ , termed Gaussian, and the other, termed the isotropic FP, with  $u_I^*(n) = \mathcal{O}[\epsilon] > 0$ . For  $d < 4$  the Gaussian FP is unstable, i.e.,  $\lambda_u^G > 0$ , so that systems for which  $u > 0$  flow towards the stable isotropic FP [31] (where  $\lambda_u^I < 0$ ) and those with  $u < 0$  flow to a region in which the mean-field analysis of the renormalized free-energy yields a first-order transition (stabilized by the positive sixth-order terms) [32, 33]. The Gaussian FP is thus identified as a tricritical point, separating between a first- and a second-order transitions.

The RG analysis of the cubic model, Eq. (2), for general  $n$  and in dimension  $d = 4 - \epsilon$  [27, 34, 35] yielded four FP's of order  $\epsilon$ : the Gaussian ( $G, u_G^* = v_G^* = 0$ ), isotropic ( $I, v_I^* = 0, u_I^* > 0$ ), decoupled Ising ( $D, u_D^* = 0, v_D^* > 0$ , for which the different  $Q_i$ 's decouple from each other and exhibit the Ising model behavior), and 'cubic' ( $C$ ) FP's. The location of the cubic FP,  $(u_C^*, v_C^*)$ , depends on the number of the order-parameter components,  $n$ : for small (large)  $n$ , it is in the lower (upper) half plane, as shown on the left (right) panel of Fig. 2. This figure [24] has been reproduced by other authors, e.g., Refs. 36–38, and included in textbooks [39]. In these references, the FP values were calculated using various approximations, but (except at lowest order in  $\epsilon$ ) the flow lines were drawn schematically. The figure shows the critical surface of the effective Hamiltonian in the  $u - v$  plane, on which  $|t| = h = 0$  and  $\xi = \infty$  [40]. At a finite (but very small)  $|t|$  the RG flow starts very close to this surface, and as the RG is iterated the flow stays close to the arrows in the figure. When the flow reaches the vicinity of a FP the system exhibits the critical exponents of that FP.

As seen in Fig. 2, the Gaussian FP is doubly unstable; both  $u$  and  $v$  are relevant in its vicinity. The decoupled FP is singly unstable, with  $u$  being relevant [24, 41]. The stability of the isotropic and cubic FP's depends on the borderline value  $n_c(3)$ . It was clear that  $2 < n_c(3) < 4$ , but different approximations yielded conflicting answers to the question whether  $n = d = 3$  is above or below  $n_c(3)$  (for the history, see Refs. 8, 36–38, 42, and 43 and references therein). For instance, a third-order  $\epsilon$ -expansion gave [24]  $n_c(3) \approx 3.128$  at  $\epsilon = 1$ . The result  $3 < n_c(d = 3)$  was also obtained by the scaling-field method [44]. If this were true then all the second order transitions cubic systems would be described by the universality class of the isotropic FP, and the cubic deviations from rotational symmetry would decay at criticality.

However, this scenario is now known to be wrong.

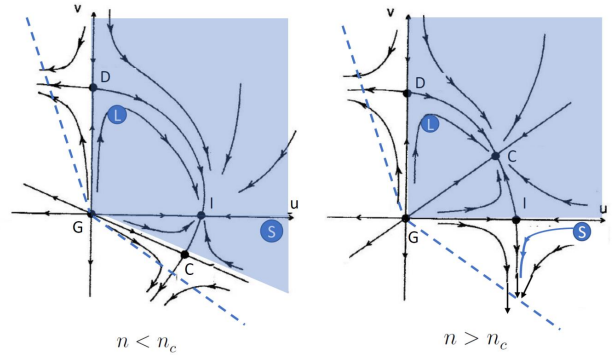


FIG. 2. (color online) Schematic flow diagram and fixed points for the cubic model, Eq. (2), adapted from Ref. 24.  $G$ =Gaussian,  $I$ =isotropic,  $D$ =Decoupled (Ising) and  $C$ =Cubic FP's.  $S$ =initial point for  $\text{SrTiO}_3$ .  $L$ =initial point for  $\text{LaAlO}_3$ . The dashed lines represent the stability edges,  $u + v = 0$  (for  $v < 0$ ) and  $u + v/n = 0$  (for  $v > 0$ ), below which the free energy in Eq. (2) is stabilized by the terms of order  $|\mathbf{Q}|^6$ , and the transitions are first-order. The shaded areas are the regions of attraction of the stable FP's ( $I$  on left and  $C$  on right).

Four accurate methods (Monte Carlo simulations of lattice  $O(n)$  models [42], six-loop recursion relations [36] at  $d = 3$ , the good old  $\epsilon$ -expansion, recently expanded to order  $\epsilon^6$  [37] and the very recent bootstrap method, which calculates exponents at any dimension [43]) find  $2.85 < n_c(3) < 3$ . Therefore, the RG flows are as in the right panel in Fig. 2: the isotropic FP is *unstable* [with a small but positive exponent for the flow of  $v$ ,  $0 < \lambda_v^I \simeq 0.02$ , see Eq. (1)], while the cubic FP has a small but positive FP value  $v_C^* > 0$ , and is fully stable (deviations of both  $u$  and  $v$  from it decay under the RG iterations).

Without even looking at the specific numerical values of the locations of the FP's, the right panel of Fig. 2 yields *qualitative* crucial consequences: since the cubic to trigonal and cubic to tetragonal transitions correspond to opposite signs of  $v$ , they have different flow trajectories. For the former,  $v < 0$ . If the initial  $|v|$  is small, and if the initial  $u$  is positive, so that  $u + v > 0$ , then the respective effective Hamiltonian (shown by the blue trajectory leaving  $S$  in Fig. 2) first flows closer to the isotropic FP, and may then exhibit  $t$ -dependent effective exponents associated with that FP, but eventually it *must* turn downwards, and cross the stability line  $u + v = 0$  - turning the transition fluctuation-driven first-order [45]. As  $\lambda_v^I$  is small at  $n = d = 3$  [36, 37, 42, 43], this flow is slow, so that the first-order transition will occur only close to  $T_c$ , with a small discontinuity. For larger initial  $|v|$ 's the transition becomes first-order at larger  $|t|$ . In contrast, the cubic to trigonal transition has  $v > 0$ , and therefore its Hamiltonian *must* flow to the stable cubic FP, resulting in a second-order transition with cubic exponents.

As mentioned above, the cubic and the isotropic FP's are close to each other at  $n = d = 3$  [36, 37, 42, 43].

Indeed, the calculated asymptotic critical exponents (expected only at very small  $|t|$ ) are  $\nu^I \simeq 0.706$ ,  $\nu^C \simeq 0.700$ ,  $\beta^I \simeq .366$ ,  $\beta^C \simeq 0.368$ . This closeness also implies that the stability exponent of the stable cubic FP,  $\lambda_3^C \lesssim 0$  and that of the unstable isotropic FP,  $\lambda_v^I \gtrsim 0$ , are small, indicating slow flows towards and away from these FP's. The experimental exponents should therefore be compared with effective exponents, e.g.,  $\beta_{\text{eff}} \equiv \partial \log |\mathbf{Q}| / \partial \log |t|$ , which depend on  $|t|$ . For  $v > 0$ , the cubic FP is stable, with two negative stability exponents,  $\lambda_4^C < \lambda_3^C < 0$  (for flows in the  $u-v$  plane). Therefore  $\beta_{\text{eff}}$  approaches the asymptotic  $\beta^C$  slowly, with corrections of order  $|t|^{\varphi_3^C}$ , where  $\varphi_3^C = \nu^C \lambda_3^C$  is small. For  $v < 0$ ,  $\beta_{\text{eff}}$  first approaches the isotropic FP value  $\beta^I$ , but then (for smaller  $|t|$ , i.e., larger number of iterations  $\ell$ ), it moves away from that value, and  $|\mathbf{Q}|$  has a discontinuity.

### III. RG FLOW NEAR THE ISOTROPIC AND CUBIC FIXED POINTS

To quantify the above qualitative statements, we used existing  $\epsilon^6$ -order expansions [37] to derive RG flow equations in the vicinity of the isotropic and cubic fixed points at  $d = n = 3$ . As discussed in Ref. 37 (and also in other references, e.g., Refs. 46–49), these series are divergent, and numerical estimates of the quantities of interest at  $\epsilon = 1$  were obtained employing resummation techniques, see Appendix A.

Critical exponents are found from the RG recursion relations for the various scaling fields. To linear order in  $\mu_i(\ell)$  these have the form

$$\frac{\partial \mu_i}{\partial \ell} = \lambda_i(\epsilon, u, v) \mu_i(\ell), \quad (4)$$

where the effective exponent  $\lambda_i$  is expanded in powers of its arguments and then resummed. At a fixed point,  $u^*$  and  $v^*$  are replaced by their  $\epsilon$ -expansions, and the series for  $\lambda_i$  are resummed to give asymptotic values at  $d = n = 3$  [37].

As mentioned,  $v$  varies slowly near the isotropic and cubic FP's. Therefore, we need to solve the recursion equations (3) as functions of the number of iterations  $\ell$ , and then estimate the effective critical exponents  $\lambda_i(\ell)$  at finite values of  $\ell$ , up to the total number of iterations  $\ell_f$ . Since  $t(\ell) = t(0)e^{\lambda_1 \ell}$ , a larger  $\ell_f$  implies a smaller  $t(0)$ , i.e., an initial state closer to the critical point. The divergence of the  $u$ - and  $v$ -dependent series for  $\beta_u$ ,  $\beta_v$  and  $\lambda_i$  prevents their use in solving the differential equations (3). Instead, we derived approximate expressions of  $\beta_u$  and  $\beta_v$ , by expanding them to second order near the isotropic FP, and resumming the  $\epsilon$ -expansions of the resulting coefficients. Since the cubic FP is expected to be close to the isotropic one, we expect these expansions

TABLE I. Numerical estimates of the coefficients entering Eqs. (5), (6) and (15). The numbers are found by means of the resummation procedure described in Appendix A.

Quantity	Value	Quantity	Value
$u_I^*$	0.39273(63)	$v_I^*$	0
$a_{01}$	-0.4791(19)	$a_{10}$	-0.7967(57)
$a_{11}$	-0.938(36)	$a_{02}$	-0.037(21)
$a_{20}$	-3.423(58)	$b_{01}$	0.0083(15)
$b_{11}$	-1.854(15)	$b_{02}$	-2.971(18)
$\beta^I$	0.3663(12)[48]	$\gamma^I$	1.385(4)[48]
$\varphi^I$	1.263(13)[49]		
$c_{10}$	0.431(17)	$c_{01}$	0.258(10)
$c_{11}$	0.49(11)	$c_{20}$	0.82(20)
$c_{02}$	0.29(11)	$d_{10}$	1.177(62)
$d_{01}$	0.706(38)	$d_{11}$	0.820(54)
$d_{20}$	1.367(90)	$d_{02}$	0.26(12)

to give reasonable results near both FP's. Hence,

$$\frac{\partial \delta u}{\partial \ell} = \lambda_u \delta u + a_{01} v + a_{11} v \delta u + \frac{1}{2} [a_{20} \delta u^2 + a_{02} v^2], \quad (5)$$

$$\frac{\partial v}{\partial \ell} = \lambda_v v + b_{11} v \delta u + \frac{1}{2} b_{02} v^2, \quad (6)$$

where  $\delta u = u - u_I^*$  and the coefficients  $a_{ij}$  and  $b_{ij}$ , which are given in Table I, are found from

$$a_{ij} = \widehat{\text{Rsm}} \left[ \frac{\partial^{(i+j)} \beta_u(u, v)}{\partial u^i \partial v^j} \right] \bigg|_{u=u_I^*, v=0},$$

$$b_{ij} = \widehat{\text{Rsm}} \left[ \frac{\partial^{(i+j)} \beta_v(u, v)}{\partial u^i \partial v^j} \right] \bigg|_{u=u_I^*, v=0}. \quad (7)$$

The operation  $\widehat{\text{Rsm}}$  denotes resummation of the  $\epsilon$  expansions at  $\epsilon = 1$  (and  $n = 3$ ) of the derivatives, using the procedure described in Appendix A. Specifically,  $\lambda_u^I \equiv \lambda_u = a_{10}$  and  $\lambda_v^I \equiv \lambda_v = b_{01}$  are the stability exponents of the isotropic FP, known accurately from resummations of the  $\epsilon^6$  series [37]. Similarly, the isotropic exponents are identical to those calculated before, e.g. in Ref. 37. The values in Table I are taken from Refs. 48 and 49, which use the same resummation as described in Appendix A.

To solve the recursion relations (5) and (6), it is convenient to define the non-linear scaling field [50, 51],

$$g_u = \delta u + z_{01} v + z_{20} \delta u^2 + z_{11} v \delta u + z_{02} v^2. \quad (8)$$

Here and below we keep only quadratic terms in  $\delta u$  and  $v$ , since the recursion relations used that approximation.

TABLE II. Numerical estimates of the cubic fixed point and the exponents obtained by our approximation, compared to those found in Ref. 37 and those calculated by means of the resummation strategy suggested in Ref. 48 and used in Appendix A. The error bars on the approximate values are based on Eq. (15).

Quantity	Effective	Ref. 37	Using Ref. 48
$u_C^*$	0.3791(27)	-	0.376(19)
$v_C^*$	0.0226(43)	-	0.028(11)
$\gamma^C$	1.3849(61)	1.368(12)	1.387(9)
$\beta^C$	0.3663(21)	0.3684(13)	0.3669(12)

Using the coefficients

$$\begin{aligned}
z_{01} &= a_{01}/(\lambda_u - \lambda_v) \approx 0.595, \\
z_{11} &= -\left(a_{11} - \frac{a_{01}a_{20}}{\lambda_u} + \frac{a_{01}b_{11}}{\lambda_u - \lambda_v}\right)/\lambda_v \approx -2.051 \\
z_{20} &= -a_{20}/(2\lambda_u) \approx -2.148, \\
z_{02} &= \frac{a_{02}/2 + a_{01}z_{11} + b_{02}z_{01}/2}{\lambda_u - 2\lambda_v} \approx -0.0983, \quad (9)
\end{aligned}$$

this scaling field obeys the linear equation

$$\frac{\partial g_u}{\partial \ell} = \lambda_u g_u, \quad (10)$$

where  $A = b_{11}g_u(0)/\lambda_u$ ,  $B = -(b_{11}/a + b_{02}/2)$  and  $\Gamma[s, z]$  is the incomplete gamma function.

Figure 3 shows the resulting RG trajectories, beginning at several initial points. We have checked that these analytic solutions coincide with a direct numerical solution of Eqs. (5)-(6) for the range shown in the figure. As seen, each RG trajectory has two (or three) main parts. In the first  $\ell_1$  iterations,  $g_u(\ell)$  decays quickly to zero, implying a fast non-universal transient flow towards the asymptotic line (12). In this part, the points at integer values of  $\ell$  are rather far from each other, indicating the fast flow. In the second part, the trajectory practically coincides with the asymptotic line. On this line, the points at integer values of  $\ell$  become dense, indicating a slow variation with  $\ell$ . For  $v > 0$ , this implies a slow approach to the cubic fixed point. For  $v < 0$ , this slow flow is followed by a third part, in which the flow gradually speeds up as the trajectory moves towards more negative values of  $v$ .

As explained in Appendix B, the flow at large  $\ell$  can be

with the solution

$$g_u(\ell) = g_u(0)e^{\lambda_u \ell}. \quad (11)$$

Since  $\lambda_u = a_{10} = -0.7967(57)$ , the exponential factor decreases fast with  $\ell$ . Indeed, we show below that after a relatively small number of iterations  $\ell_1 = \ln[\delta/g_u(0)]/\lambda_u$ , with, say  $g_u(\ell_1) = \delta = 10^{-3}$ , during which the RG trajectories undergo a transient non-universal flow, the trajectories approach a universal asymptotic line, on which they either flow to the cubic fixed point [ $v(0) > 0$ ] or to the first order region [ $v(0) < 0$ ]. Examples of solutions are shown in Fig. 3, where the asymptotic line is shown in red. This figure should replace the schematic Fig. 2 near the isotopic and cubic fixed points.

The explicit solution of the differential equations is presented in Appendix B. We first express  $\delta u(\ell)$  in terms of  $g_u(\ell)$  and  $v(\ell)$ , from Eq. (8). Since  $g_u(\ell)$  quickly decays to zero, after a relatively small number of iterations  $\ell_1$ , the flow quickly approaches an asymptotic line,

$$\begin{aligned}
\delta u(\ell) &\rightarrow -z_{01}v(\ell) - [z_{02} + z_{01}^2 z_{20} - z_{01}z_{11}]v(\ell)^2 \\
&\approx -.595v - .3613v^2. \quad (12)
\end{aligned}$$

This line is *universal*, since its coefficients are fully determined by the isotropic fixed point. Keeping terms up to quadratic order in  $g_u(\ell)$  and  $v(\ell)$  yields a single differential equation, with the solution

$$\frac{1}{v(\ell)} = e^{-Ae^{\lambda_u \ell}} e^{-\lambda_v \ell} \left[ \frac{e^A}{v(0)} + \frac{(-A)^{-\lambda_v/\lambda_u} B}{\lambda_u} \left( \Gamma[\lambda_v/\lambda_u, -A] - \Gamma[\lambda_v/\lambda_u, -Ae^{\lambda_u \ell}] \right) \right], \quad (13)$$

described by

$$v(\ell) = \frac{v(\ell_1)e^{\lambda_v(\ell-\ell_1)}}{1 + Bv(\ell_1)[e^{\lambda_v(\ell-\ell_1)} - 1]/\lambda_v}. \quad (14)$$

Since  $\lambda_v$  is very small, the variation of the second term in the denominator with  $\ell$  is slow, explaining the second part above.. Since  $B = 0.3706 > 0$ , this implies a slow variation in  $v$  for positive  $v$ , approaching the cubic fixed point  $v_C^* = \lambda_v/B$ . However, for  $v(0) < 0$   $v(\ell)$  becomes more negative. At first it decreases slowly, but when  $e^{\lambda_v \ell}$  becomes of order unity this decrease becomes faster (the points at integer  $\ell$  become less dense), and  $v(\ell)$  diverges at  $\ell = \ell_2$ , when  $[e^{\lambda_v(\ell_2-\ell_1)} - 1]/\lambda_v \approx \ell_2 - \ell_1 = -1/[Bv(\ell_1)]$ . This value is larger for smaller  $|v(\ell_1)|$  [and therefore also for smaller  $|v(0)|$ ]. Within our quadratic approximation, we are not allowed to follow this solution beyond some finite value, say  $v < -.2$ . However, it is reasonable that a full solution will also continue downwards, on the asymptotic trajectory, and reach the first order transition at  $v(\ell) = -u(\ell)$ .

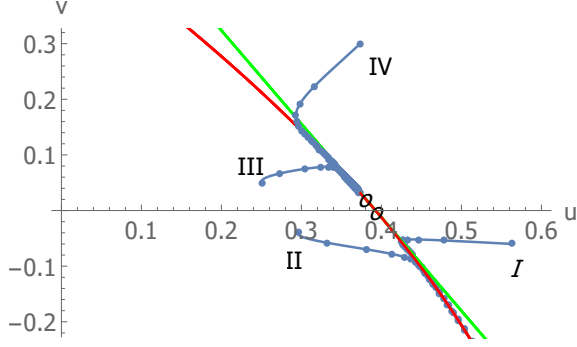


FIG. 3. (color online) Flow trajectories in the  $u-v$  plane (blue) for several initial points. The dots indicate integer values of  $\ell$ . The red line is the universal asymptotic line, Eq. (12). The green line is the asymptotic line in the linear approximation,  $v = -\delta u/z_{01}$ . The small circles denote the isotropic ( $v_I^* = 0$ ) and cubic fixed points.

The effective critical exponents  $\beta$  and  $\gamma$  are given by

$$\begin{aligned} \beta(u, v) &= \beta^I + c_{10}\delta u + c_{01}v + c_{11}v\delta u + \frac{c_{20}}{2}\delta u^2 + \frac{c_{02}}{2}v^2, \\ \gamma(u, v) &= \gamma^I + d_{10}\delta u + d_{01}v + d_{11}v\delta u + \frac{d_{20}}{2}\delta u^2 + \frac{d_{02}}{2}v^2, \end{aligned} \quad (15)$$

with the coefficients listed in Table I. Figure 4 shows these effective exponents, calculated with  $v(\ell)$  and  $\delta u(\ell)$  from Eqs. (13) and (B2). As expected, the exponents with  $v(0) > 0$  (dashed lines) approach the asymptotic values of the cubic fixed point (which are practically the same as those of the isotropic one). The rate of these approaches depends on the initial value  $g_u(0)$ , and the corresponding effective exponents are smaller (larger) than the asymptotic ones if  $g_u(0) < 0$  ( $> 0$ ). Both trajectories I and IV in Fig. 3 have  $g_u(0) > 0$ , and therefore both start at similar large effective exponents, and reach the vicinity of the isotropic (=cubic) fixed point values after a few iterations ( $\ell_1 \sim 5$ ). Generally, each value of  $\ell$  is related to the initial value of  $t$  via  $t(\ell) \sim t(0)e^{\ell/\nu}$ . Assuming that the RG iterations end after  $\ell_f$  iterations, when  $t(\ell_f) \sim 1$ , the asymptotic exponents can be observed only if  $|t(0)| < e^{-\ell_f/\nu} \sim e^{-5/\nu} \sim 10^{-3}$ . Trajectories II and III start at similar negative values of  $g_u(0)$ , and therefore they both approach the asymptotic lines from below, resulting with effective exponents smaller than the asymptotic isotropic ones. After reaching the asymptotic line, the flow on that line is slow. For trigonal systems, with  $v(0) > 0$ , the effective exponents vary slowly on that line until they approach the asymptotic cubic values.

In the tetragonal case,  $v(0) < 0$ , the beginning of the trajectories is similar to that described above, depending only on the sign of the initial  $g_u(0)$ , which is not universal. Once the asymptotic line is reached, the initially slow growth of  $|v|$ , causes the effective exponents to approach slowly (mostly below) the isotropic asymptotic values, but then they turn downwards, diverging at

a value  $\ell = \ell_2$  that depends on the value of  $v(\ell_1)$ . Since the decrease in the exponents in part 3 of the flow is fully determined by the flow on the universal asymptotic line, and depends only on  $v(\ell_1)$ , one can collapse the two full curves in Fig. 4 onto each other just by shifting them along the  $\ell$  axis. In particular, the decreasing part of line of curve I accurately overlaps that of line II when we shift  $\ell \rightarrow \ell - 15$ . This reflects a universality of these effective exponents. We are not aware of earlier discussions of such a universality.

We stopped our calculation when the trajectory left the region  $|v| < 0.2$ , where our quadratic approximation may fail. However, we expect that the asymptotic universal line will eventually cross the line  $v = -u$ , and the transition will become first order. Given Eq. (14), this will happen at larger  $\ell$ , i.e., smaller  $t$ , when  $|v(0)|$  is smaller. Since  $\text{SrTiO}_3$  is supposed to have a very small negative  $v$  (see below), this may explain why its first order transition happens at a very small  $t$ , which has not yet been reached experimentally. In contrast,  $\text{KMnF}_3$  and  $\text{RbCaF}_3$  do show first order transitions at some finite  $t$ , implying that they start at larger values of  $|v(0)|$ .

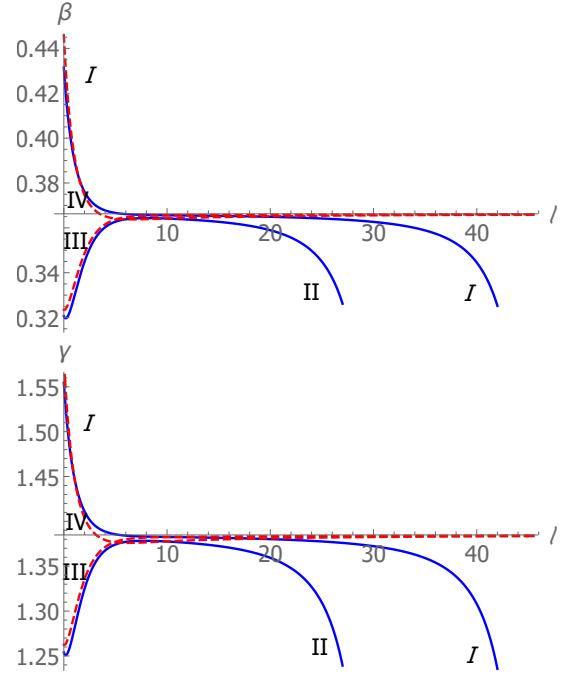


FIG. 4. (color online) Effective exponents  $\beta$  and  $\gamma$  for the trajectories shown in Fig. 3, as functions of  $\ell$ . The horizontal axes are at the asymptotic values of the isotropic fixed point (which are also very close to those at the cubic fixed point). The exponents corresponding to trajectories with  $v(0) > 0$  (III and IV, dashed lines) approach this asymptotic value. In contrast, those with  $v(0) < 0$  (I and II, full lines) initially come close to these values, but then turn downwards, diverging at

## IV. EXPERIMENTS

Based on the mean-field region of the experiments, Müller *et al.* [52] estimated the ‘initial’ Landau parameters to be  $\{u, v\}_S \cong \{1.91, -0.068\}$  for  $\text{SrTiO}_3$  and  $\{u, v\}_L \cong 0.06 \pm 0.06, 0.68 \pm 0.06\}$  for  $\text{LaAlO}_3$ , all in cgs units divided by  $10^{43}$ . These rough values (which should be improved!) fit beautifully with our expectations:  $\text{SrTiO}_3$  (S in Fig. 2) has a small initial negative  $v$ , and we predict that it will flow quickly parallel to the horizontal axis towards the universal asymptotic line and the isotropic FP before turning downwards, as for trajectory I in Fig. 3.

On the other hand,  $\text{LaAlO}_3$  (L in Fig. 2) starts close to the positive  $v$ -axis, in a region which is probably not covered by our quadratic approximation. In principle, one could perform an expansion of the RG recursion relations near the decoupled Ising fixed point. Since the instability exponent at that fixed point,  $\lambda_u^D = \alpha^D/\nu^D$  (with the Ising values of  $\alpha$  and  $\nu$  [24]) is small, we again expect two parts for the flows which begin close to the  $v$ -axis. At first, the trajectories will flow quickly to the vicinity of the decoupled fixed point, dominated by the large negative exponent  $\lambda_v^D$  (=the stability exponent of the Ising FP), approaching a universal asymptotic line on which they will flow slowly away from the decoupled FP. Eventually, this asymptotic line will coincide with the one we calculated near the isotropic FP, and the flows will approach the cubic fixed point along that line, as in trajectories III and IV in Fig. 4. Interestingly, the line (12) reached the  $v$ -axis at  $v \approx 0.5$ , quite close to the decoupled FP value  $v_D^* = 0.482(9)$  which we calculated for  $n = 1$  using the resummation technique of Appendix A. Therefore, Eq. (12) may give a good approximation for the whole universal line connecting the D, C and I fixed points.

To the best of our knowledge, there are no experiments showing first-order transitions into the trigonal phase [53], but – as listed in Sec. I – several experiments found such transitions into the tetragonal phase. Interestingly, the experiments listed in Sec. I exhibit intermediate regions (before the first-order transitions) with effective critical exponents, which are smaller than their isotropic values. This is consistent with our Fig. 4. The smaller values of  $\beta$  in  $\text{NaNbO}_3$  have also been attributed to the inter-plane weak correlations along the rotation axis [54].

To test our predictions in detail, we propose a repeated analysis of existing experiments, and new dedicated experiments, in which the critical exponents will be measured over several separate ranges of  $t$ , to check how they vary with  $t$  (which is equivalent to their dependence on the number of iterations  $\ell$ ).

As mentioned in Sec. I, polishing the surfaces of the crystals  $\text{SrTiO}_3$  and  $\text{LaAlO}_3$  caused a crossover from the  $n = 3$  critical behavior to that of the Ising ( $n = 1$ ) critical behavior. This crossover is due to an axially anisotropic Hamiltonian,  $\mathcal{H}_g^{\alpha\beta} = g(Q_\alpha Q_\beta - \delta_{\alpha\beta} \mathbf{Q}^2/3)$ , where  $g$  rep-

resents the uniaxial stress. Such uniaxial stress has also been applied directly, yielding information on the corresponding exponent  $\lambda_g$ . Existing experiments gave a range of values for  $\lambda_g$ . A detailed application of our theory to these exponents will be presented separately.

One way to vary  $v$  experimentally is to use mixed crystals, e.g.  $\text{Sr}_{1-x}\text{Ca}_x\text{TiO}_3$  [55] or a mixture of  $\text{SrTiO}_3$  with  $\text{LaAlO}_3$ , which is expected to be easy to grow due to their matching lattice constants [2]. Since both the isotropic and cubic FP’s have  $d\nu > 2$ , randomness is irrelevant [56, 57] and one expects the same competition predicted above. It is interesting to note that  $\text{KMn}_{1-x}\text{Ca}_x\text{F}_3$  seems to approach a second-order transition as  $x$  increases [58]. If the transition is still into the tetragonal structure, this may represent a smaller value of the initial  $|v|$  in the dilute case. This may be caused by the larger dimension of the parameter space in the dilute case, which involves many transient iterations until the flow reaches the  $u - v$  plane [57].

Three-component order-parameter vectors  $\mathbf{Q}$  with cubic symmetry are abundant. Examples include ferroelectric transitions from cubic to tetragonal or trigonal, ferromagnets and antiferromagnets with the magnetization ordering along an axis or a diagonal. Close to their transitions, these cubic crystals may be described by Eq. (2), and therefore their critical behavior is expected to split into the two types described above. In particular, *ordering of the  $n = 3$  cubic system along a cube axis must be fluctuation-driven first-order, with intermediate effective isotropic exponents!* This important prediction can be tested experimentally [59].

## V. CONCLUSIONS

In conclusion, we have shown that for systems having cubic symmetry, universality is not determined merely by the symmetry above the transition. Rather, the critical behavior of such systems depends on their symmetry *below* the transition. Cubic systems split into two groups – those that become trigonal, which belong to the cubic FP universality class, and those that become tetragonal, which undergo a fluctuation driven first-order transition. In both cases, there is a wide temperature range in which slow-varying effective exponents, which exhibit universal features, are expected. For systems like  $\text{SrTiO}_3$ , the cubic to tetragonal transition exhibits effective exponents close to those of the isotropic FP, but then cross over to a fluctuation-driven first-order transition. This crossover is accompanied by large changes in the effective exponents, which await experimental detection. These results resolve a long standing confusion about the universality of the displacive phase transitions in the perovskites, and leaves its complete confirmation to future dedicated experiments, concentrating on the  $t$ -dependence of the effective exponents.

## ACKNOWLEDGMENTS

This research was initiated by a very stimulating discussion with Slava Rychkov, who drew our attention to the new accurate values of  $n_c$  (see also Ref. 8). A.K. gratefully acknowledges Mikhail Kompaniets for the helpful discussion and Andrey Pikelner for his help with RG expansions from Ref. 60, and the support of Foundation for the Advancement of Theoretical Physics "BASIS" through Grant 18-1-2-43-1.

## Appendix A: Details of the resummation

Since the  $\epsilon$ -expansions, e.g.  $f(\epsilon) = \sum_{k=0}^{\infty} f_k \epsilon^k$ , are divergent, numerical estimates of the quantities of interest at  $d = 3$  are obtained employing proper resummation techniques [46, 47]. Such resummations were performed for the isotropic and cubic FP's in Ref. 37, which used the basic resummation procedure of the Padé-Borel-Leroy method. Here we use the  $\epsilon$ -expansions based on those in Ref. 37, but apply the more advanced resummation strategy proposed in Ref. 48. The main idea of this strategy can be formulated simply: the asymptotic behavior of the series coefficients for large order is written as

$$f_k \xrightarrow[k \rightarrow \infty]{} c k! k^{b_0} (-a)^k, \quad (\text{A1})$$

where  $1/a$  is the radius of convergence and  $b_0$  is fixed by the high-order asymptotic behavior of the series. How-

ever, in practice we only have a limited number of terms in the series, and consequently this asymptotic behavior is not known. Therefore, the authors of Ref. 48 proposed to treat the Leroy parameter  $b = b_0 + 3/2$  as a free parameter, to be determined variationally (see below).

Once a Borel transformation, based on this modified asymptotic form, is performed, the variable  $\epsilon$  is conformally mapped onto

$$w(\epsilon) = \frac{\sqrt{1+a\epsilon} - 1}{\sqrt{1+a\epsilon} + 1}, \quad \epsilon(w) = \frac{4w}{a(1-w)^2}, \quad (\text{A2})$$

and it is assumed that the function has the strong asymptotic behavior  $f(\epsilon) \sim \epsilon^\lambda$ ,  $\epsilon \rightarrow \infty$ . The results are then improved by a preliminary homogeneous homographic transformation,

$$\epsilon(\epsilon') \rightarrow \frac{\epsilon'}{1+q\epsilon'}, \quad \epsilon'(\epsilon) \rightarrow \frac{\epsilon}{1-q\epsilon}, \quad (\text{A3})$$

and the final approximate estimates are found by applying the steps mentioned above to the new  $\epsilon'$  expansion. Finally, the optimal values of the parameters  $b$ ,  $\lambda$  and  $q$  (for each series) are determined by the least sensitivity to their variation (for details see Ref. 48). This technique was applied to find all the coefficients listed in Table I.

## Appendix B: Solution of the differential equations

Solving Eq. (8) for  $\delta u(\ell)$  yields

$$du(\ell) = \left[ -1 - z_{11}v(\ell) + \sqrt{[1 + z_{11}v(\ell)]^2 - 4z_{20}[z_{01}v(\ell) + z_{02}v(\ell)^2 - g_u(\ell)]} \right] / (2z_{20}). \quad (\text{B1})$$

Expanding to quadratic order in  $v(\ell)$  and  $g_u(\ell)$  gives

$$\delta u(\ell) \approx g_u(\ell) - z_{20}g_u(\ell)^2 - [z_{01} + (z_{11} - 2z_{01}z_{20})g_u(\ell)]v(\ell) - [z_{02} + z_{01}^2z_{20} - z_{01}z_{11}]v(\ell)^2. \quad (\text{B2})$$

After a few iterations  $g_u(\ell)$  decays to zero, and this solution reaches the asymptotic line (12).

We now return to Eq. (6). Substituting Eq. (B2), and stopping at quadratic order, this equation becomes

$$\begin{aligned} \frac{\partial v}{\partial \ell} &\approx \lambda_v v(\ell) + b_{11}[g_u(\ell) - z_{01}v(\ell)]v(\ell) + b_{02}v(\ell)^2/2 \\ &= \lambda_v v(\ell) + b_{11}g_u(\ell)v(\ell) - Bv(\ell)^2, \end{aligned} \quad (\text{B3})$$

where  $B \equiv b_{11}z_{01} - b_{02}/2$ . This can be written as

$$\frac{\partial}{\partial \ell} \left[ \frac{1}{v} \right] = -[\lambda_v + b_{11}g_u(0)e^{\lambda_u \ell}] \left[ \frac{1}{v} \right] + B. \quad (\text{B4})$$

To solve this equation, we write  $x = e^{\lambda_u \ell}$  and

$$\frac{1}{v(x)} = e^{-Ax} x^{-\lambda_v/\lambda_u} W(x), \quad (\text{B5})$$

where  $A = b_{11}g_u(0)/\lambda_u$ . This yields

$$\frac{dW}{dx} = \frac{B}{\lambda_u} e^{Ax} x^{\lambda_v/\lambda_u - 1}, \quad (\text{B6})$$

with the solution (13), where

$$\Gamma[s, z] = \int_z^\infty t^{s-1} e^{-t} dt. \quad (\text{B7})$$

is the incomplete gamma function.

For large  $\ell$ ,  $x = e^{\lambda_u \ell}$  is small, and  $\Gamma[s, z] = -z^s/s + \mathcal{O}[1]$ , so that  $\Gamma[\lambda_v/\lambda_u, -Ax] \propto e^{\lambda_v \ell}$ . This result can be

obtained directly: For  $\ell > \ell_1$  we can neglect  $g_u(\ell)$  in Eq. (B4). The solution to this equation is then given in Eq. (14).

- 
- [1] F. Dogan, H. Lin, M. Guilloux-Viry and O. Peña, *Focus on properties and applications of perovskites*, *Sci. Technol. Adv. Mater.* **16**, 020301 (2015).
  - [2] e.g., A. Ohtomo and H. Hwang, *A high-mobility electron gas at the LaAlO<sub>3</sub>/SrTiO<sub>3</sub> heterointerface*, *Nature* **427**, 423 (2004).
  - [3] J. D. Axe and M. K. Crawford, *Structural instabilities in lanthanum cuprate superconductors*, *J. Low Temp. Phys.* **95**, 271 (1994).
  - [4] K. A. Müller and W. Berlinger, *Static critical exponents at structural phase transitions*, *Phys. Rev. Lett.* **26**, 13 (1971).
  - [5] A. Aharony and A. D. Bruce, *Polycritical points and flop-like displacive transitions in Perovskites*, *Phys. Rev. Lett.* **33**, 427 (1974).
  - [6] K. A. Müller and W. Berlinger, *Behavior of SrTiO<sub>3</sub> near the [100]-stress-temperature bicritical point*, *Phys. Rev. Lett.* **35**, 1547 (1975).
  - [7] A. D. Bruce and A. Aharony, *Coupled order parameter, symmetry breaking irrelevant scaling fields and tetracritical points*, *Phys. Rev. B* **11**, 478 (1975).
  - [8] The history of the interplay between theory and experiments following this exchange, and a preliminary report of the present results, were recently reviewed in three lectures by A. Aharony, at [Bootstat 2021: Conformal Bootstrap and Statistical models](#), Paris, May 2021.
  - [9] K.A. Müller and J. C. Fayet, *Structural phase transitions studied by electron paramagnetic resonance*, in Ref. 18, Vol. II, p. 1.
  - [10] F. Borsa and A. Rigamonti, *Comparison of NMR and NQR studies of phase transitions in disordered and ordered crystals*, in Ref. 18, Vol. II, p. 83.
  - [11] G. O'Ariano, S. Aldrovandi, and A. Rigamonti, *Critical behavior of the order parameter at antiferrodistortive transitions with cubic fluctuations*, *Phys. Rev. B* **25**, 7044 (1982).
  - [12] P. R. Garnier, *Specific heat of SrTiO<sub>3</sub> near the structural transition*, *Phys. Lett.* **35A**, 413 (1971).
  - [13] J. O. Fossum, K. Fossheim and H. J. Scheel, *Ultrasonic investigation of the phase transition in flux-grown SrTiO<sub>3</sub>*, *Solid State Comm.* **51**, 839 (1984).
  - [14] E. K. H. Salje, M. C. Gallardo, J. Jiménez, F. J. Romero and J. del Cerro, *The cubic-tetragonal phase transition in strontium titanate: excess specific heat measurements and evidence for a near tricritical, mean field type transition mechanism*, *J. Phys.: Condens. Matter* **10**, 5535 (1998).
  - [15] M. Hikada, S. Maeda and J. S. Storey, *Structural phase transitions of RbCaF<sub>3</sub>*, *Phase Transitions* **5**, 219 (1985).
  - [16] S. Stokka and K. Fossheim, *Specific heat and phase diagrams for uniaxially stressed KMnF<sub>3</sub>*, *J. Phys. C: Solid State Phys.* **15**, 1161 (1982).
  - [17] R. Pynn and A. Skjeltorp, eds., **Multicritical Phenomena**, *Proc. NATO advanced Study Institute series B, Physics*; Vol. 106, Plenum Press, NY 1984.
  - [18] K. A. Müller and H. Thomas, eds., **Structural phase transitions I**, and **Structural phase transitions II** (Springer-Verlag Berlin, 1991).
  - [19] R. A. Cowley, *The Phase Transition of Strontium Titanate*, *Phil. Trans.: Math., Phys. and Eng. Sci.* **354**, 2799 (1996).
  - [20] K. G. Wilson, *The renormalization group and critical phenomena* (1982, Nobel Prize Lecture), *Rev. Mod. Phys.* **55**, 583 (1983).
  - [21] K. G. Wilson and J. Kogut, *The renormalization group and the  $\epsilon$  expansion*, *Phys. Rep.* **12**, 75 (1974).
  - [22] M. E. Fisher, *The renormalization group in the theory of critical behavior*, *Rev. Mod. Phys.* **46**, 597 (1974).
  - [23] M. E. Fisher, *Renormalization group theory: Its basis and formulation in statistical physics*, *Rev. Mod. Phys.* **70**, 653 (1998).
  - [24] A. Aharony, *Dependence of universal critical behavior on symmetry and range of interaction*, in **Phase Transitions and Critical Phenomena**, C. Domb and M. S. Green, eds., Vol. 6 (Academic Press, NY, 1976), pp. 357-424.
  - [25] L. D. Landau and E. M. Lifshitz, **Statistical Physics**, (Pergamon, 1994).
  - [26] J.-C. Tolédano, P. Tolédano, **The Landau Theory of Phase Transitions**, (World Scientific, Singapore, 1987).
  - [27] A. Aharony, *Critical behavior of anisotropic cubic systems*, *Phys. Rev. B* **8**, 4270 (1973).
  - [28] J. C. Slonczewski and H. Thomas, *Interaction of Elastic Strain with the Structural Transition of Strontium Titanate*, *Phys. Rev. B* **1**, 3599 (1970).
  - [29] V. L. Ginzburg and L. D. Landau, *Zh. Eksp. Teor. Fiz.* **20**, 1064 (1950). English translation in: L. D. Landau, *Collected papers* (Oxford: Pergamon Press, 1965), p. 546.
  - [30] K. G. Wilson and M. E. Fisher, *Critical Exponents in 3.99 Dimensions*, *Phys. Rev. Lett.* **28**, 240 (1972), K. G. Wilson, *Feynman-Graph Expansion for Critical Exponents*, *Phys. Rev. Lett.* **28**, 548 (1972).
  - [31] e.g., A. D. Bruce and D. J. Wallace, *Crossover behaviour and effective critical exponents in isotropic and anisotropic Heisenberg systems*, *J. Phys. A: Math. Gen.* **9**, 1117 (1976).
  - [32] J. Rudnick and D. R. Nelson, *Equations of state and renormalization-group recursion relations*, *Phys. Rev. B* **13**, 2208 (1976); J. Rudnick, *First-order transition induced by cubic anisotropy*, *Phys. Rev. B* **18**, 1406 (1978).
  - [33] D. Blankschtein and A. Aharony, *Crossover from Fluctuation-Driven Continuous Transitions to First-Order Transitions*, *Phys. Rev. Lett.* **47**, 439 (1981).
  - [34] R. A. Cowley and A. D. Bruce, *Application of the Wilson theory of critical phenomena to a structural phase transition*, *J. Phys. C: Solid State Phys.* **6**, L191 (1973).
  - [35] I. J. Kettle and D. J. Wallace, *A modified  $\epsilon$  expansion for a hamiltonian with cubic point-group symmetry*, *J. Phys. A: Math. Nucl. Gen.* **6**, 1667 (1973).
  - [36] J. M. Carmona, A. Pelissato and E. Vicari, *N-Component Ginzburg-Landau Hamiltonians with cubic anisotropy: A*

- six-loop study*, *Phys. Rev. B* **61**, 15136 (2000).
- [37] L. T. Adzhemyan, E. V. Ivanova, M. V. Kompaniets, A. Kudlis, and A. I. Sokolov, *Six-loop  $\epsilon$  expansion study of three-dimensional  $n$ -vector model with cubic anisotropy*, *Nucl. Phys. B* **940**, 332 (2019). The detailed coefficients of the  $\epsilon$  expansions appear in the Ancillary files of arXiv:1901.02754.
- [38] For a review, see A. Pelissetto and E. Vicari, *Critical phenomena and renormalization-group theory*, *Phys. Rep.* **368**, 542 (2002).
- [39] e.g. P. M. Chaikin and T. C. Lubensky, **Principles of Condensed Matter Physics**, (Cambridge University Press, 1995); J. Cardy, **Scaling and Renormalization in Statistical Physics**, Cambridge University press, 1996); M. Kardar, **Statistical physics of fields**, (Cambridge University press 1997).
- [40] At  $t = 0$ , the correlation length diverges,  $\xi = \infty$ , and the flow stays on the  $u - v$  plane. For a finite sample, the cutoff  $\xi$  in Eq. (1) is replaced by the system's linear size,  $L$ . Macroscopic quantities, like the average order-parameter, are then powers of  $L$ , e.g.  $|\mathbf{Q}| \propto L^{-\beta/\nu}$ . This is the basis for finite-size scaling.
- [41] A. Aharony, *Comment on "Bicritical and tetracritical phenomena and scaling properties of the  $SO(5)$  theory"*, *Phys. Rev. Lett.* **88**, 059703 (2002); *Old and new results on multicritical points*, *J. Stat. Phys.* **110**, 659 (2003).
- [42] M. Hasenbusch and E. Vicari, *Anisotropic perturbations in three-dimensional  $O(N)$ -symmetric vector models*, *Phys. Rev. B* **84**, 125136 (2011).
- [43] S. M. Chester, W. Landry, J. Liu, D. Poland, D. Simmons-Duffin, N. Su and A. Vichi, *Bootstrapping Heisenberg magnets and their cubic anisotropy*, *Phys. Rev. D* **104**, 105013 (2021).
- [44] E. Domany and E. K. Riedel, *Study of cubic anisotropy in three dimensions by the scaling-field method*, *J. of Appl. Phys.* **50**, 1804 (1979).
- [45] E. Domany and M. E. Fisher, *Equations of state for bicritical points. III. Cubic anisotropy and tetracriticality*, *Phys. Rev. B* **15**, 3510 (1977).
- [46] E. Brézin, J. C. Le Guillou, and J. Zinn-Justin, *Perturbation theory at large order. I. The  $\phi^{2N}$  interaction*, *Phys. Rev. D* **15**, 1544 (1977).
- [47] L. N. Lipatov, *Divergence of the perturbation-theory series and the quasi-classical theory*, *Soviet Physics JETP* **45**, 216 (1977).
- [48] M. V. Kompaniets, and E. Panzer, *Minimally subtracted six-loop renormalization of  $O(n)$ -symmetric  $\phi^4$  theory and critical exponents*, *Phys. Rev. D* **96**, 036016 (2017).
- [49] M. V. Kompaniets, and K. J. Wiese, *Fractal dimension of critical curves in the  $O(n)$ -symmetric  $\phi^4$  model and crossover exponent at 6-loop order: Loop-erased random walks, self-avoiding walks, Ising, XY, and Heisenberg models*, *Phys. Rev. E* **101**, 012104 (2020).
- [50] A. Aharony and M. E. Fisher, *Universality in Analytic Corrections to Scaling for Planar Ising Models*, *Phys. Rev. Lett.* **45**, 679 (1980); Erratum *Phys. Rev. Lett.* **45**, 1044 (1980).
- [51] The non-linear scaling field may also contain other irrelevant parameters, e.g., the coefficients of the sixth order terms in  $U_0[\mathbf{Q}(\mathbf{r})]$  and in  $U_v[\mathbf{Q}(\mathbf{r})]$ , see Ref. 33. These affect only the non-universal initial  $g_u(0)$  and  $v(0)$ .
- [52] K.A. Müller, W. Berlinger, J.E. Drumheller and J.G. Bednorz, *Bi- and Tetra-critical Behaviour of Uniaxially Stressed  $LaAlO_3$* , in Ref. 17, p. 143.
- [53] In fact, experiments on  $LaAlO_3$  indicate a second order transition: S. A. Hayward, F. D. Morrison, S. A. T. Redfern, E. K. H. Salje, J. F. Scott, K. S. Knight, S. Tarantino, A. M. Glazer, V. Shuvaeva, P. Daniel, M. Zhang, and M. A. Carpenter, *Transformation processes in  $LaAlO_3$ : Neutron diffraction, dielectric, thermal, optical, and Raman studies*, *Phys. Rev. B* **72**, 054110 (2005).
- [54] A. Aharony and A. D. Bruce, *Lifshitz-point critical and tricritical behavior in anisotropically stressed perovskites*, *Phys. Rev. Lett.* **42**, 462 (1979) and references therein; J. Y. Buzaré, J. C. Fayet, W. Berlinger and K. A. Müller, *Tricritical behavior of uniaxially stressed  $RbCaF_3$* , *Phys. Rev. Lett.* **42**, 465 (1979) Similar phenomena were also observed for uniaxially stressed  $KMnF_3$  [S. Stokka and K. Fossheim, *Specific heat and phase diagrams for uniaxially stressed  $KMnF_3$* , *J. Phys. C: Solid State Phys.* **15**, 1161 (1982)].
- [55] B. S. de Lima et al., *Interplay between antiferrodistortive, ferroelectric and superconducting instabilities in  $Sr_{1-x}Ca_xTiO_{3-\delta}$* , *Phys. Rev. B* **91**, 045108 (2015).
- [56] A. B. Harris, *Effect of random defects on the critical behaviour of Ising models*, *J. Phys. C: Solid State Phys.* **7**, 1671 (1974).
- [57] A. Aharony, *Critical behavior of amorphous magnets*, *Phys. Rev. B* **12**, 1038 (1982).
- [58] W. Schranz, P. Sondergeld, A. V. Kityk, and E. K. H. Salje, *Dynamic elastic response of  $KMn_{1-x}Ca_xF_3$ : Elastic softening and domain freezing*, *Phys. Rev. B* **80**, 094110 (2009).
- [59] The distinction between ordering along an axis or along a diagonal was already noticed in Ref. 38. Here we emphasize the variation of the effective exponents for both cases, and the large variations of these exponents in the latter fluctuation-driven first-order case.
- [60] A. Bednyakov, and A. Pikelner, *Six-loop beta functions in general scalar theory*, *J. High Energ. Phys.* **2021**, 233 (2021).